

shows gains of -37.31 , -27.09 , and -30.18 dB, respectively. And one can see from Fig. 11(c) that gains are less than -22.5 dB at all of these three directions. Therefore, the results obtained by the piecewise integration CFDTD method show better agreement with experimental data.

V. CONCLUSION

A continuous long slot leaky-wave antenna is presented in this paper that illustrates the freedom of design introduced by this new approach. And the design scheme has been tested experimentally in *Ka* band. And good agreement between simulated and measured data has been observed.

REFERENCES

- [1] S. W. Lü *et al.*, "The technique for design of long slot antenna on cam-rectangular wave guide," *Chinese Aeronautical Sci Technol Rep*, 1996, HJB961475.
- [2] K. S. Yee, "Numerical solutions of initial boundary value problems involving Maxwell's equations in isotropic media," *IEEE Trans. Antennas Propag.*, vol. 14, pp. 302–307, May 1966.
- [3] S. Dey and R. Mittra, "A locally conformal finite-difference time-domain (FDTD) algorithm for modeling three-dimensional perfectly conducting objects," *IEEE Microw. Guided Wave Lett.*, vol. 7, pp. 273–275, Sep. 1997.
- [4] W. Yu and R. Mittra, "A conformal FDTD software package modeling antennas and microstrip circuit components," *IEEE Antennas Propag. Mag.*, vol. 42, pp. 28–38, Oct. 2000.
- [5] T. Xiao and Q. H. Liu, "Enlarged cells for the conformal FDTD method to avoid the time step reduction," *IEEE Microw. Wireless Compo. Lett.*, vol. 14, pp. 551–553, Dec. 2004.
- [6] W. Tang *et al.*, "A new FDTD conform technique for scattering analysis," *J. Xidian Univ.*, vol. 32, pp. 290–293, Apr. 2005.
- [7] W. B. Dou and E. K. N. Yung, "Spectrum change of Gaussian pulse in waveguide by FDTD method," in *Proc. Asia-Pacific Microwave Conf.*, 2000, pp. 1001–1004.

An Accurate Model for Rectangular Trifurcated Horns

Kwok Kee Chan and Sudhakar Rao

Abstract—An accurate model of the *n*-furcated horn in general and a trifurcated horn in particular is presented. This type of horn is frequently used as a feed for reflector antennas in communication satellites. It is relatively lightweight and has low sidelobes and cross-polar levels. The horn is divided into four regions—a flared transformer, an enlarged *n*-furcated guide, long flare partitioned guides, and an *n*-furcated guide to aperture junction. A modal analysis of the horn is carried out to obtain the aperture modal content, which is used to compute accurately the radiated fields. The measurements and predictions of the amplitude and phase patterns of a trifurcated horn at the 4/6 GHz band show excellent agreement.

Index Terms—Generalized scattering matrix, Horn antennas, mode matching methods, reflector antenna feeds.

I. INTRODUCTION

There is a need for a linear polarized radiator that has radiation patterns with possibly different E-plane and H-plane beamwidths to

Manuscript received January 18, 2007; revised July 27, 2007.

K. K. Chan is with Chan Technologies Incorporated, Brampton, ON L6Y 5H1, Canada (e-mail: Kwok-kee.chan@rogers.com).

S. Rao is with the Lockheed Martin Commercial Space Systems, Newtown, PA 18940 USA.

Color versions of one or more of the figures in this paper are available online at <http://ieeexplore.ieee.org>.

Digital Object Identifier 10.1109/TAP.2007.910502

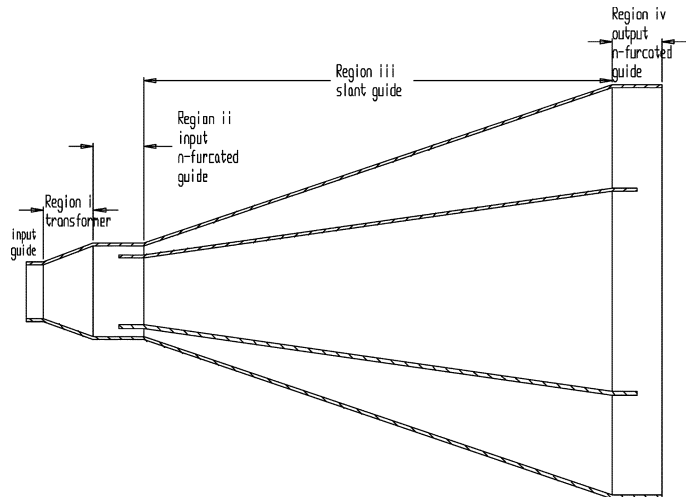


Fig. 1. Side view of the trifurcated horn.

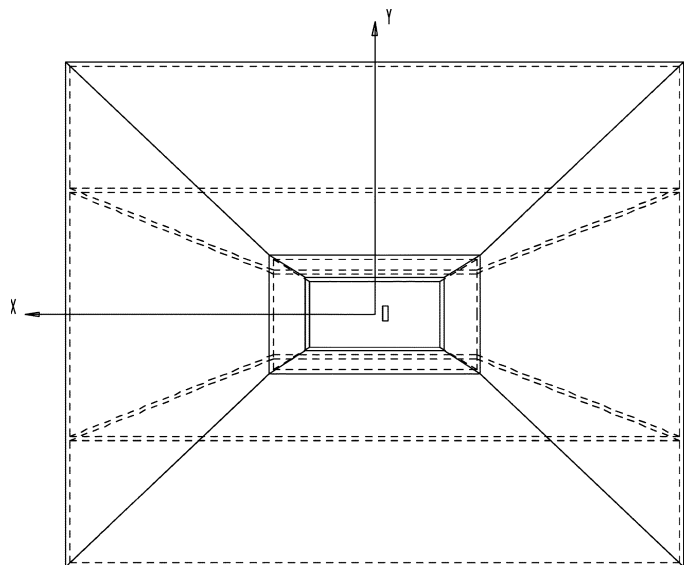


Fig. 2. End view of the trifurcated horn.

illuminate a shaped reflector for fixed satellite service (FSS) applications at the *C*- and *Ku*-band frequencies. Such feeds are required to have large bandwidths of about 66% (especially at *C*-band), low sidelobe levels to minimize the spillover losses, and extremely low cross-polar levels for frequency re-use. The circular or elliptical corrugated horn is capable of fulfilling such requirements but it is expensive to manufacture and is very large and heavy, especially for frequencies below *X*-band. It is well known that for a normal corrugated horn designed for dual band operation such as 4/6 GHz, the cross-polar performance is very good at the low band but deteriorates at the high band because the corrugation depth is approaching half-wavelength thereby modifying the optimum aperture modal content. This may be overcome by using dual-depth or ring-loaded corrugations, which in either case leads to an increase in weight and weight is a prime consideration for satellite applications. The alternative is to use a trifurcated horn [1], [2], where two metallic plates are inserted into a rectangular horn to create a tapered amplitude distribution in the E-plane. This together with the cosine distribution in the H-plane will produce a pattern with low sidelobes in all planes. Further, a peak cross-polarization level of less than -40 dB relative to copolar peak

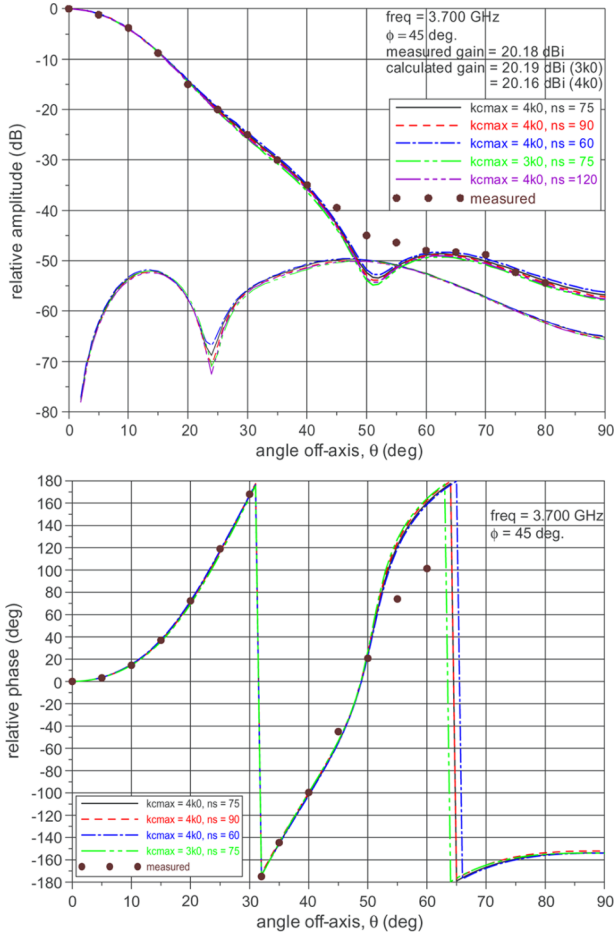


Fig. 3. Amplitude and phase patterns in the diagonal plane at 3.700 GHz.

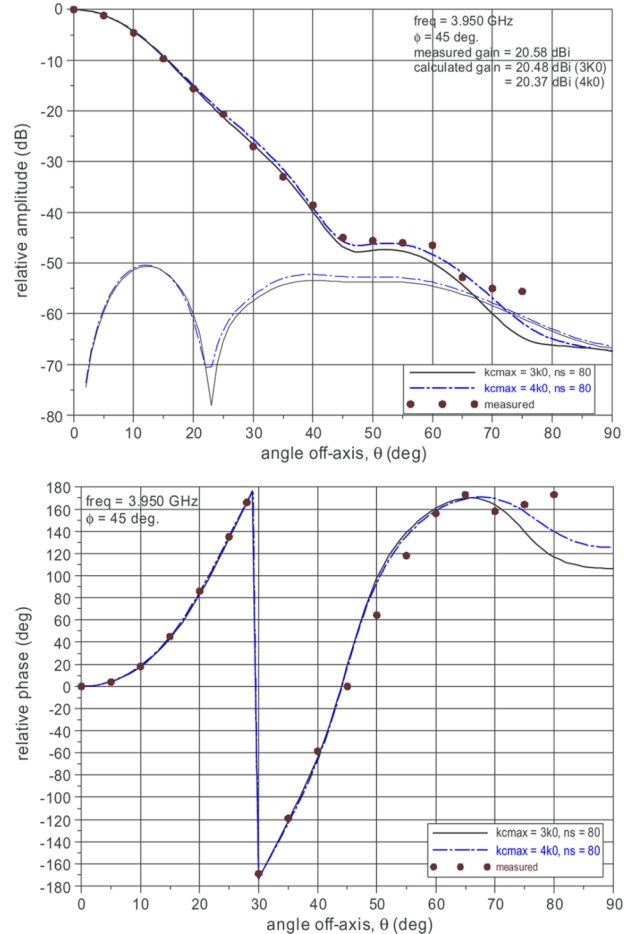


Fig. 4. Amplitude and phase patterns in the diagonal plane at 3.950 GHz.

gain can be easily achieved by the trifurcated horn over a very broad-band. Such type of horn has thin wall construction. Hence it is much lighter in weight and can be spaced closer together in a multiple-horn environment, as compared to the corrugated horn. Thus it is well suited for use in satellite antennas as a single feed or in a feed array.

Previously, the prediction of the radiation patterns of the trifurcated horn was based on an assumed relative amplitude excitation of the three apertures, with each aperture taking on the field distribution of the TE₁₀ mode. The radiated fields from these apertures are combined to give the resultant far-field pattern. This simplified theory does not account for the coupling between the apertures or the discontinuities at the furcated junction and flared guides nor the dividing plate thickness. Hence, the input match of the horn is not calculated, and the computed amplitude and phase patterns differ from those measured. For shaping of reflectors, accurate amplitude and phase feed patterns are necessary for obtaining a first-time-right design.

The present analysis method makes use of mode matching method [3]–[5] to characterize each discontinuity of the horn by means of a generalized scattering matrix. The generalized scattering matrices are then combined together to completely describe the behaviour of the horn. This development takes into account the coupling between the guides at the input and the aperture furcated junctions. Consequently, both the amplitude and phase patterns as well as the input match are accurately predicted. They have been verified by extensive comparisons with measured results of a C-band horn from Lockheed Martin [6].

II. ANALYSIS OF A RECTANGULAR TRIFURCATED HORN

Side and end view drawings of a trifurcated horn are shown in Figs. 1 and 2, respectively. The horn is made up of four regions. Region i is

the input matching section that is either stepped or flared, as depicted in Fig. 1, from the input guide into a waveguide with a larger cross-section. The power splitting is done in a larger waveguide as it will lead to better input match and more accurate amplitude distribution. Region ii is an E-plane trifurcated guide with H-plane partitions to provide the appropriate power split. Typically, the E-plane dimensions of the trifurcated guides at the input are in the ratio of 1:8:1. The guide dimensions of Region ii are such that the first symmetrical TE/TM₁₂ or TE₃₀ modes are still evanescent. If the former pair is excited, they will become trapped modes and if the latter is generated, it will affect the aperture H-plane distribution. The thicknesses of the plates are accounted for in our model. In Region iii, the trifurcated guides flare out to larger E- and H-plane dimensions. Each furcated guide is modeled as a series of stepped sections, where they may or may not overlap, depending on the direction of the flare. In the case where the sections overlap, an extra guide of zero length is introduced in-between the two overlapping guides. The cross section of this in-between guide is enclosed entirely within that of the adjacent guides. The metallic walls partition the aperture area in the ratio of 1:2:1 in Region iv. This will result in amplitude excitations of the three sub-apertures in the ratio 1:2:1. In Region iv, the trifurcated guides terminate into a rectangular guide with a cross section equal to that of the aperture. The length of the aperture guide section may be set to zero.

The analysis of the horn is carried out using the mode matching technique that was well documented in [3]–[5]. Typically, the field at each waveguide cross section is represented by a series of mode functions. At a discontinuity, matching of the tangential electric and magnetic fields of the incident and reflected waves leads to a generalized scattering matrix (GSM) description of that junction. The GSMs of the

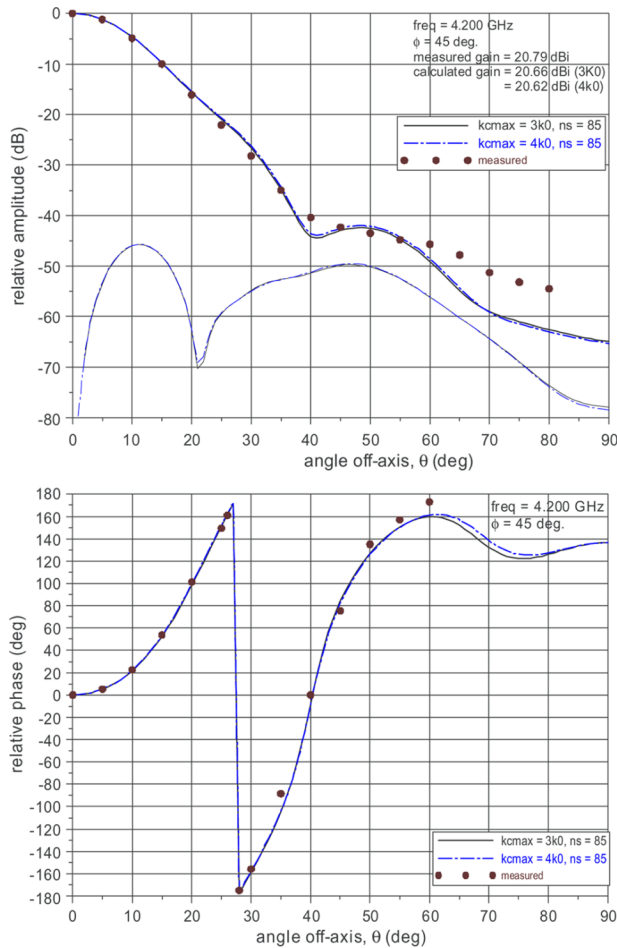


Fig. 5. Amplitude and phase patterns in the diagonal plane at 4.200 GHz.

various junctions making up the horn are combined together to yield an overall scattering matrix characterization. In Region ii, the coupling between the partitioned guides and the input feed guide are fully taken into account. Similarly, in Region iv, the coupling between the furcated guides and the aperture are also included in the analysis. This is done by attaching a length of waveguide between the partitions and the aperture in Region iv. It will result in an additional furcated waveguide junction. The length of this guide may be set to zero. Typically, the aperture size is of a few wavelengths. The reflection from the aperture/free space boundary is negligible and hence neglected here. For the pattern computation, the aperture is surrounded by an infinite ground plane. Knowing the modal content of the aperture, the near field diffraction integral is numerically computed to give the co-polarized and cross-polarized gain values at any observation angle and distance, for instance, at the reflector surface points. The accuracy of this model is fully validated by both amplitude and phase measurements.

III. COMPARISON BETWEEN PREDICTED AND MEASURED RESULTS

The validation of the above model is carried out using a C-band trifurcated horn that was developed by Lockheed Martin. This horn has an aperture with E- and H-plane dimensions of 11.54 and 14.0 inches and sub-apertures of 2.875×14 inches and 5.75×14 inches. The axial lengths of Region i, ii, iii, and iv are 1.720, 0, 23.28, and 0 inches respectively. The dividing plates are 0.063 inch thick but they taper down to 0.020 inch at the feed and aperture ends starting about 0.75 inch away. The input guide has dimensions of 0.844 by 1.771 inches. Both

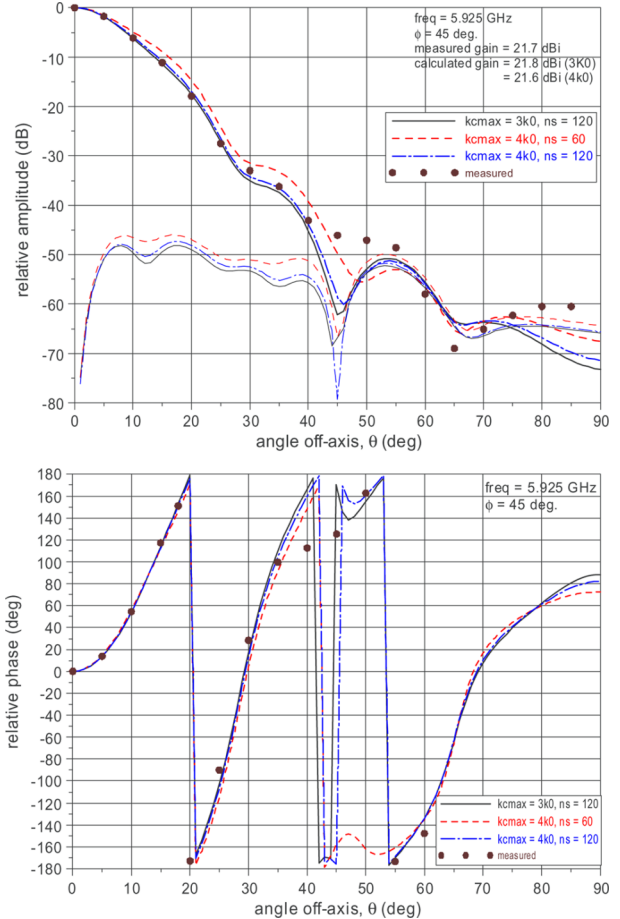


Fig. 6. Amplitude and phase patterns in the diagonal plane at 5.925 GHz.

measured amplitude and phase patterns are compared with the predictions at frequencies over the 4/6 GHz band. These comparisons are shown in Figs. 3–8. Also shown on these plots are the patterns resulting from different number of approximating modes and number of sections to represent the flare guides of Region iii. Very close agreement is obtained between measurements and predictions in all the amplitude and phase patterns compared. The correlation is excellent between boresight and out to the region where the amplitude has dropped below -45 dB. This is the critical region as this portion of the beam is used to illuminate the reflector. Also the cross-polar level in the diagonal plane is very low, below -40 dB. A convergence investigation was carried out to determine the number of modes needed. The variable k_{cmax} is the highest cutoff wave number of the modes used to approximate the field distribution at each discontinuity. It is sufficient to set $k_{cmax} = 3k_0$ to obtain convergence. This will result in 457 modes at the aperture guide section at 3.7 GHz, of which only 48 modes are propagating. Also the number of sections, ns , used to represent the smooth flare guide of Region iii must be such that the size of the step between sections must be less than 0.035λ . Further the computed boresight gains agree very well with the measured values over the 4/6 GHz band as seen in Table I. The predicted input return loss of the horn is listed in Table II showing that the horn is well matched. At 5.925 GHz, with $k_{cmax} = 3k_0$, the number of modes approximating the field distribution at the aperture is 1155 and 129 of these modes are propagating. The analysis on a Dell Precision 650 containing an Intel Xeon processor operating at 2.8 GHz took 15 min. With $k_{cmax} = 4k_0$, the number of aperture modes increases to 2040 and the runtime required 93 min.

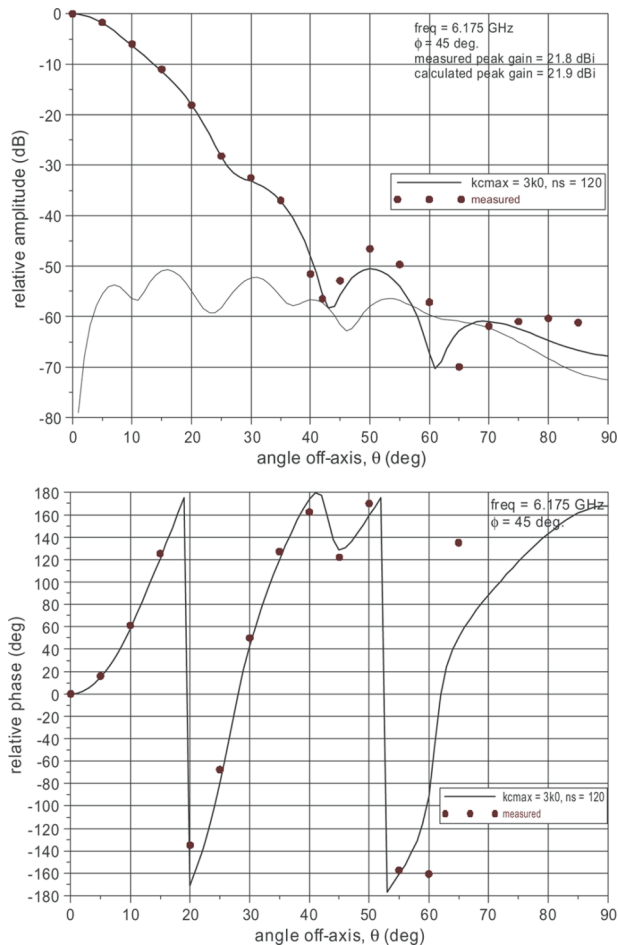


Fig. 7. Amplitude and phase patterns in the diagonal plane at 6.175 GHz.

TABLE I
ON-AXIS GAIN OF THE TRIFURCATED HORN

Frequency (GHz)	Computed (dBi)	Measured (dBi)
3.700	20.16	20.18
3.925	20.37	20.58
4.200	20.62	20.79
5.925	21.60	21.70
6.175	21.90	21.80
6.425	21.80	21.90

The efficiency of the horn is about 52% at 3.7 GHz and 26% at 5.925 GHz. The reasons for the low efficiency are that the aperture distribution is tapered to produce low sidelobes, and secondly the phase distribution is not uniform as can be seen from Figs. 3–7. For contoured beam applications, the efficiency of the primary horn is not important but the high taper and low cross polar illumination of the reflector is critical. This type of horn is therefore ideally suited for such satellite communication applications.

IV. CONCLUSION

We have demonstrated that the trifurcated horn possesses both low sidelobes and cross polar levels through analysis and measurements.

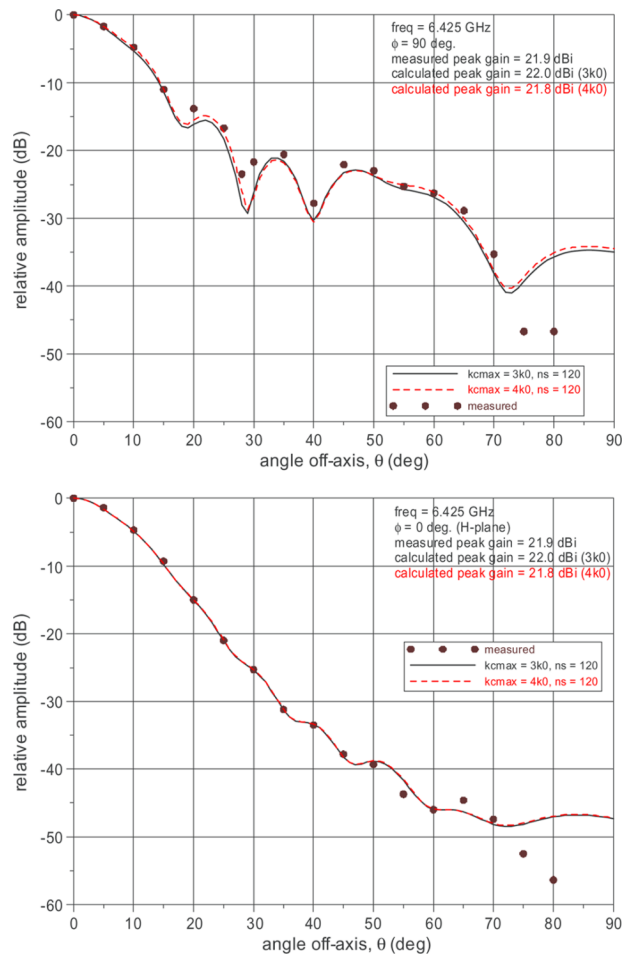


Fig. 8. E- and H- plane amplitude patterns at 6.425 GHz.

TABLE II
INPUT MATCH OF THE TRIFURCATED HORN

Frequency (GHz)	Computed Input Return loss (dB)
3.700	-22.50
3.950	-35.46
4.200	-37.67
5.925	-24.57
6.175	-24.64
6.425	-24.42

These desirable features combined with its light weight construction make the horn an excellent linearly polarized feed for the reflector antenna in satellite communications. The analysis method is useful for the design of the flight horns without the need for breadboard and could be useful for establishing manufacturing tolerances.

REFERENCES

- [1] G. M. Peace and E. E. Swartz, "Amplitude compensated horn antenna," *Microw. J.*, vol. 7, pp. 66–68, 1964.
- [2] K. K. Chan, C. C. Huang, and A. R. Raab, "Dielectric-loaded trifurcated horn for H-plane stacked reflector feed array," *Proc. Inst. Elect. Eng.*, vol. 127, no. 1, pt. H, pp. 61–64, Feb. 1980.
- [3] G. L. James, "Analysis and design of TE₁₁ to HE₁₁ corrugated cylindrical waveguide mode converter," *IEEE Trans. Microw. Theory Tech.*, vol. 29, no. 10, pp. 1059–1066, Oct. 1981.

- [4] J. Dittloff and F. Arndt, "Rigorous field theory design of millimetre-wave E-plane integrated circuit multiplexers," *IEEE Trans. Microw. Theory Tech.*, vol. 37, no. 2, pp. 340–350, Fe. 1989.
- [5] A. D. Olver *et al.*, *Microwave Horns and Feeds ser. IEE Electromagnetic Wave Series 39*, ch. 4, 1994.
- [6] K. K. Chan and S. Rao, "Modal analysis of trifurcated horn," in *Proc. IEEE AP-Symp.*, Albuquerque, NM, Jul. 2006, pp. 3157–3160.

Epsilon Negative Zeroth-Order Resonator Antenna

Jae-Hyun Park, Young-Ho Ryu, Jae-Gon Lee, and Jeong-Hae Lee

Abstract—It is confirmed that zeroth-order resonance appears in the epsilon negative (ENG) meta-structured transmission line (MTL) as well as in the conventional double negative (DNG) MTL. The zeroth-order resonant characteristics are described using dispersion relation of ENG MTL based on Bloch and Floquet theory. Applying the novel concept of the ENG zeroth-order resonator (ZOR), an ENG ZOR antenna is proposed. The radiation characteristics of the ZOR antennas using the DNG and ENG MTL are simulated and measured, and are proven to be the same.

Index Terms—Double negative transmission line (DNG TL), epsilon negative transmission line (ENG TL), zeroth-order resonator (ZOR).

I. INTRODUCTION

The planar meta-structured transmission line is a consequence of extraordinary permittivity and permeability. As it is known well, the double negative (DNG) meta-structured transmission line (MTL) is composed of unit cells with a series capacitance and a shunt inductance based on conventional transmission line. The series capacitance and the shunt inductance provide the left-handed propagation characteristic which supports the backward wave [1], [2]. Also, the DNG MTL has right-handed propagation property because the DNG MTL has inevitable series inductance and shunt capacitance of the conventional transmission line. More importantly, the DNG MTL has unique property of an infinite wavelength wave at specific non-zero frequency where permittivity and permeability are zero. Various applications using the infinite wavelength wave such as power divider [3], zeroth-order resonator (ZOR) [4], and ZOR antenna [5], [6] have been reported.

In this paper, it is suggested that the ENG MTL as well as the DNG MTL supports the zeroth-order resonance mode. The ENG MTL with series inductance and shunt inductance provides the epsilon negative bandstop region and the right-handed region. At the boundary of ENG bandstop region and the right-handed region, the ENG MTL has the zeroth-order resonant mode because the ENG MTL has zero permittivity. The zeroth-order resonance of the ENG MTL will be demonstrated using the infinitesimal circuit model and compared with that of the DNG MTL. It will be shown that the ENG ZOR and DNG ZOR have the same zeroth-order resonance frequency where a permittivity of each

Manuscript received January 27, 2007; revised July 17, 2007. This work was supported by the Seoul R&BD Program.

J.-H. Park, J.-G. Lee, and J.-H. Lee are with the Department of Electronic Information and Communication Engineering, Hongik University, Seoul 121-791, Korea (e-mail: jeonglee@hongik.ac.kr).

Y.-H. Ryu is with the School of Electrical Engineering and Computer Science, Kyungpook National University, Daegu 702-701, Korea.

Color versions of one or more of the figures in this paper are available online at <http://ieeexplore.ieee.org>.

Digital Object Identifier 10.1109/TAP.2007.910505

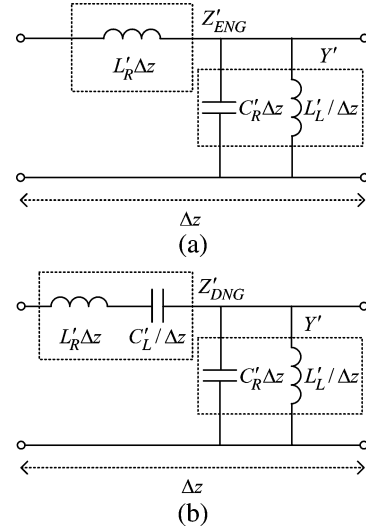


Fig. 1. Infinitesimal circuit model. (a) ENG MTL and (b) DNG MTL (Z'_{ENG} , Z'_{DNG} , and Y' are the per-unit length impedance and admittance).

ZOR is zero. Consequently, the ENG ZOR antenna can be easily implemented because the series capacitance of the DNG ZOR antenna is removed. Finally, the ZOR antennas using a 3-stage ENG and DNG ZOR will be presented and their radiation characteristics will be compared.

II. THEORY

An infinitesimal circuit models of lossless ($R = 0$ and $G = 0$) artificial ENG and DNG MTL are expressed as shown in Fig. 1. The ENG MTL model can be represented as the combination of a per-unit length series inductance (L'_R), shunt capacitance (C'_R), and a times-unit length shunt inductance (L'_L) as shown in Fig. 1. The DNG MTL model is represented by adding a times-unit length series capacitance (C'_L) to the ENG MTL circuit. According to lossless transmission line theory, the propagation constant of a TL is given by $\gamma = j\beta = \sqrt{Z'Y'}$, where Z' and Y' are the per-unit length impedance and admittance, respectively. The effective permeability and permittivity of the MTL materials based on expression of $\beta = \omega\sqrt{\mu\epsilon}$ are obtained as [6]

$$\begin{aligned} \mu_{\text{ENG}} &= \frac{Z'_{\text{ENG}}}{j\omega} = L'_R, & \mu_{\text{DNG}} &= \frac{Z'_{\text{DNG}}}{j\omega} = L'_R - \frac{1}{\omega^2 C'_L} \\ \epsilon_{\text{ENG}} &= \epsilon_{\text{DNG}} = \frac{Y'}{j\omega} = C'_R - \frac{1}{\omega^2 L'_L}. \end{aligned} \quad (1)$$

When the frequency band is satisfied with $\omega < 1/\sqrt{L'_R C'_L}$ and $\omega < 1/\sqrt{L'_L C'_R}$, the DNG MTL has double negative passband because of simultaneously negative permeability and permittivity. If the frequency band is to be $\omega < 1/\sqrt{L'_L C'_R}$, the ENG MTL has single negative stopband because of positive permeability and negative permittivity. The ENG and DNG MTLs have unique characteristic of an infinite-wavelength wave which appears at the boundary of passband and stopband of non-zero frequency. A propagation constant of MTLs can be obtained by applying the Bloch and Floquet theory to the unit cell as follows,

$$\begin{aligned} \beta_{\text{ENG}} d &= \cos^{-1} \left\{ 1 - \frac{1}{2} \left(\frac{\omega^2 - \omega_E^2}{\omega_R^2} \right) \right\} \\ \beta_{\text{DNG}} d &= \cos^{-1} \left\{ 1 - \frac{1}{2} \left[\frac{\omega_L^2}{\omega^2} + \frac{\omega^2}{\omega_R^2} - \left(\frac{\omega_E^2}{\omega_R^2} + \frac{\omega_M^2}{\omega_R^2} \right) \right] \right\} \end{aligned} \quad (2)$$

where $\omega_R = 1/\sqrt{L'_R C'_R}$, $\omega_L = 1/\sqrt{L'_L C'_L}$, $\omega_M = 1/\sqrt{L'_R C'_L}$, and $\omega_E = 1/\sqrt{L'_L C'_R}$. β is a phase constant for Bloch waves, and d is length of the unit cell. C'_R , L'_R , C'_L , and L'_L are the series capacitance,